Received: 21 October 2021 | Revised: 17 January 2022 | Accepted: 19 January 2022

DOI: 10.1002/btpr.3237

RESEARCH ARTICLE

BIOTECHNOLOGY PROGRESS

Particle-based analysis elucidates the real retention capacities of virus filters and enables optimal virus clearance study design with evaluation systems of diverse virological characteristics

Taiki Kayukawa[1] | Akiyo Yanagibashi[2] | Tomoko Hongo-Hirasaki[3] | Koichiro Yanagida[3]

[1]Medical Technology & Material Laboratory, Research and Business Development Division, Asahi Kasei Medical Co., Ltd., Shizuoka, Japan

[2]Bioprocess Technical Development Division, Asahi Kasei Medical MT CORP., Miyazaki, Japan

[3]Bioprocess Division, Asahi Kasei Medical Co., Ltd., Miyazaki, Japan

Correspondence
Taiki Kayukawa, Medical Technology & Material Laboratory, Research and Business Development Division, Asahi Kasei Medical Co., Ltd., Fuji, Shizuoka, Japan.
Email: kayukawa.tb@om.asahi-kasei.co.jp

Abstract

In virus clearance study (VCS) design, the amount of virus loaded onto the virus filters (VF) must be carefully controlled. A large amount of virus is required to demonstrate sufficient virus removal capability; however, too high a viral load causes virus breakthrough and reduces log reduction values. We have seen marked variation in the virus removal performance for VFs even with identical VCS design. Understanding how identical virus infectivity, materials and operating conditions can yield such different results is key to optimizing VCS design. The present study developed a particle number-based method for VCS and investigated the effects on VF performance of discrepancies between apparent virus amount and total particle number of minute virus of mice. Co-spiking of empty and genome-containing particles resulted in a decrease in the virus removal performance proportional to the co-spike ratio. This suggests that empty particles are captured in the same way as genome-containing particles, competing for retention capacity. In addition, between virus titration methods with about 2.0 Log_{10} difference in particle-to-infectivity ratios, there was a 20-fold decrease in virus retention capacity limiting the throughput that maintains the required LRV (e.g., 4.0), calculated using infectivity titers. These findings suggest that ignoring virus particle number in VCS design can cause virus overloading and accelerate filter breakthrough. This article asserts the importance of focusing on virus particle number and discusses optimization of VCS design that is unaffected by virological characteristics of evaluation systems and adequately reflect the VF retention capacity.

KEYWORDS
minute virus of mice, particle to infectivity ratio, virus filter, virus filtration, virus retention capacity

1 | INTRODUCTION

Biological products are at risk of viral contamination through the introduction of adventitious agents during the manufacturing process as well as from raw materials, including cells and blood plasma.[1] To mitigate this risk, virus removal and/or inactivation procedures are incorporated into the manufacturing process to ensure the absence of viral contamination in the final product. Prior to clinical phases and

commercial production, manufacturers are required to perform viral clearance studies (VCS) using scaled-down models of actual manufacturing processes to evaluate their virus removal capability. The virus removal performance of various process steps is evaluated by adding (spiking) a model virus into actual process solutions and comparing the quantity of virus present before and after the process to determine removal efficiency.[2,3]

One method of virus removal is filtration using a virus filters (VF).[4] In designing VCS regarding virus filtration, the load of virus spiked onto the filter is important. While a high enough amount of virus must be loaded to show sufficient virus removal capability, loading too much virus can result in reduced or inconsistent virus log reduction value (LRV).[5,6] This phenomenon is known as virus overloading.

VF remove viruses based on the principle of size exclusion[7]; thus, evaluations of the virus removal performance of filtration processes often use particularly small viruses, which are the most challenging to remove. Parvoviruses are used as specific and nonspecific model viruses in many VCS of filtration processes due to their small size.[2] In most cases, the parvoviruses used in VCS are produced and titrated by methods specific to the facility performing the VCS; therefore, virus quality and its titration can vary significantly.

The effect of virus preparation quality on VCS results has been discussed.[8] The main focus of virus quality control to date has been the concentration of impurities in the virus stock. Spiking impurities contained in the virus stock along with virus into the product can cause filter fouling and decreased flux.[9] Attention is required to ensure that the spiked virus does not dilute or change the characteristics of the product. The concentration of impurities in the virus stock should be low enough that VF flux is not impacted.[2]

Another important aspect of virus quality is the virological characteristics of parvovirus capsids, including the presence or absence of a DNA genome and infectivity in cultured cells.[10,11] Parvovirus particles with encapsidated genomic DNA are called genome-containing particles or full capsids (FC) while those that lack genomic DNA are referred to as empty particles or empty capsids (EC). Genome-containing particles can be further divided into 'infectious' and 'noninfectious,' while in case of parvovirus, most genome-containing particles are considered infectious.

These virological characteristics in combination with the virus detection method alter the 'apparent virus amount'. For example, quantitative testing using genomic DNA as an index does not detect empty particles while the same virus titrated differently depending on protocols in infectivity assay. Although this variability in virus characteristics and evaluation are recognized as potential problems within the biopharmaceutical industry, their impacts on VCS are considered to be modest and no quantitative studies have been reported to date.[8,12]

However, the impact of such topics on virus removal performance should also be discussed since inconsistency in the apparent virus amount can promote virus overloading. As the physiochemical properties of these virus particles are nearly identical,[13] a virus removal method involving physical capture should equally retain all particle types. Nevertheless, any loading and subsequent removal of empty and noninfectious particles in the target process are unrecognized in conventional VCS using infectivity assays. In other words, empty and noninfectious particles are not taken into consideration when evaluating the virus removal performance of VF despite their potential to accelerate filter breakthrough. Misidentification of viral load due to infectivity may cause unintentional overloading.

Currently, industry evaluations of virus removal performance are conducted almost exclusively by infectivity assay. Empty particles and variation in infectivity assay methods potentially impact these evaluations.

The present study developed a particle number-based method for VCS and quantitatively analyzed the impact of discrepancies between infectivity titer and total particle number on evaluation of VF performance. Changes in interpretation depending on the virological characteristics of the virus stock and the virus detection methods are comprehensively discussed.

2 | MATERIALS AND METHODS

2.1 | Cells and viruses

A9 mouse fibroblast cells (CCL-1.4, purchased from ATCC) were cultured in Dulbecco's modified Eagle's medium (DMEM) supplemented with 10% fetal bovine serum (FBS) at 37°C under a 5% CO_2 atmosphere. NB324K simian virus 40-transformed human newborn kidney cell lines (purchased from Yale University) were cultured in DMEM supplemented with 5% FBS at 37°C under a 5% CO_2 atmosphere. Minute virus of mice prototype strain (MVMp) purchased from ATCC (VR-1346) was propagated in NB324K cells. Crude virus stocks were recovered from the culture supernatant of MVM-infected cells. In short, NB324K cells were infected with MVM at multiplicity of infection (MOI) 0.01 and cultured until onset of cytopathic effect. The culture medium was exchanged with serum-free DMEM and cultured for an additional 3–4 days. After removal of cell debris by low-speed centrifugation, MVM suspended in serum-free media (MVM-SF) were collected.

2.2 | Virus titration by infectivity assay

The infectivity of MVM was measured and expressed as 50% tissue culture infective dose per ml ($TCID_{50}$/ml). Both A9 and NB324K cells were used for virus titration. Initial cell densities in 96 well plates were 2.0×10^3 cells/well for A9 and 2×10^4 cells/well for NB324K. All infectivity assays are performed by ten-fold serial dilutions. The Spearman-Kärber method was used to calculate $TCID_{50}$/ml at 8 and 10 days postinfection (DPI) for A9 and NB324K, respectively. Infectivity titers are indicated as averages of triplicate results for stock virus samples and results of single titration for filtration samples. For samples showing cytotoxicity, cell culture supernatant was exchanged with fresh media at one DPI, after infection was established.

2.3 | Virus quantification by quantitative polymerase chain reaction

Template DNA was extracted using the high pure viral nucleic acid kit (Roche Diagnostics K.K.) according to manufacturer's protocols following nuclease treatment for nonencapsidated DNA digestion and subsequent nuclease inactivation. Amplification and real-time detection of quantitative polymerase chain reaction (qPCR) products were performed using a Light Cycler 96 system (Roche). Primers and fluorescent probe for MVM DNA amplification were as follows: forward primer, 5′-CTCCACTTGCATCGGATCTC-3′ (nucleotides 2053–2072); forward primer (specifically for VF samples), 5′-AGTGGTCAGAATAG GCTGCG-3′ (1730–1749); reverse primer, 5′-GGGCTCAGTTGACC ATCTTG-3′ (2169–2188); and probe, 5′-(FAM) CCCGCAACAGGAGT ATTTGGTGTGCT (BHQ1)-3′ (2097–2122).

Ten-fold serial dilutions of double strand MVM genome (159–4933, 4775 bp) were used to obtain standard curves. For plasmid cloning, amplified MVM genome fragment was inserted into pT7Blue-2 T-Vector (Novagen, Inc.). MVM genome cloned plasmid was amplified in *Escherichia coli* and digested by SalI-HF and EcoNI (NEW ENGLAND BioLabs Inc.). Standard DNA copy number was calculated from absorbance 260 nm.

2.4 | Hemagglutination assay

Hemagglutination (HA) assay was performed with chicken red blood cells (RBC) in phosphate-buffered saline (PBS) (−). Aliquots 100 μL of PBS-washed and 0.125% v/v-diluted RBC were added to two-fold serial dilutions of the samples and incubated for 1.5 h at room temperature (25°C).

2.5 | Virus purification

For MVM stock preparation used in the experiment shown in Figure 1, MVM-SF were pelleted by ultracentrifugation (29,400 rpm; Type 45 Ti Rotor; Beckman Coulter, Inc.) and resuspended in TNE buffer (50 mM Tris, 100 mM NaCl, 1 mM EDTA; pH 7.4). The ultracentrifuged MVM (MVM-UC) was purified by sucrose step gradient (40%–60%) centrifugation (103,900 × *g*; SW28; Beckman Coulter).

To produce MVM-full capsid (MVM-FC) and -empty capsid (MVM-EC) stocks used in the experiments shown in Figure 2-7, MVM-UC were further concentrated by polyethylene glycol (PEG) precipitation (10% PEG 6000, 500 mM NaCl) and resuspended in the MVM storage buffer (50 mM Tris, 10 mM $CaCl_2$, 5 mM $MgCl_2$; pH 8.0). Then, MVM were treated with micrococcal nuclease. Separation of FC and EC was performed by centrifugation (35,000 rpm; SW41; Beckman Coulter) through discontinuous iodixanol (OptiPrep; Axis-Shield, Oslo, Norway) gradients, as previously described.[14,15] Fractions were collected from the top surface of the gradient into 12 aliquots and viral capsids and DNA-containing particles in the fractions were comprehensively detected by HA assay, western blotting, and qPCR.

Fractions for FC and EC were loaded onto Zeba™ Spin Desalting Columns, 40 K MWCO (Thermo Fisher Scientific Inc.) equilibrated with MVM storage buffer and MVM was recovered from the flow-through fraction according to manufacturer's protocol. After buffer exchange, fractions for FC were treated with micrococcal nuclease followed by repeated buffer exchange (summarized in Figure 2a).

2.6 | Antibodies, enzymes, and virus-like particles

Western blotting was performed using MVMVP21-S (Alpha Diagnostic Intl. Inc.) as primary and Goat anti-Rabbit IgG (H + L) Secondary Antibody, HRP (Thermo Fisher Scientific) as secondary antibodies. All antibodies were diluted by PBS-T (dilution factor, 1:5000). Immunofluorescence (IF) microscopy of VF membranes was performed using a monoclonal antibody produced by hybridoma cells derived from inactivated-MVMp-immunized mouse as primary and Alexa Fluor Plus 488-conjugated Goat anti-Mouse IgG polyclonal antibody (Thermo Fisher Scientific) as secondary antibodies (primary and secondary antibody dilution factors, 1:1000 and 1:100, respectively).

Micrococcal nuclease (New England Biolabs) and Benzonase (MilliporeSigma) were used for pre-qPCR nuclease treatment at doses of 2000 and ≥ 25 units/reaction, respectively. Nucleases and the MVM storage buffer were added to samples and incubated for 1 h at 37°C. After incubation, 15 mM EDTA was added to stop the reaction.

MockV mock virus particles (MVPs, Cygnus Technologies) were used as model MVM empty capsids (MVM virus-like particles [MVM-VLP]). The concentration of MVM-VLP was measured by HA assay using MVM-FC copy number as a quantification standard.

2.7 | Virus filters

The 0.001m^2 of Planova 20N and Planova 15N (Asahi Kasei Medical Co., Ltd.) were used as main filters and 0.01 m^2 of Planova 35N (Asahi Kasei Medical Co., Ltd.) was used for the prefilter to remove impurities such as MVM aggregates.

2.8 | Virus filtration

All filtrations were performed in dead-end mode under constant pressure at room temperature. Filtration pressure was 78.4 kPa for Planova 20N and 15N, and 49.0 kPa for Planova 35N. For virus filtrations, MVM and/or VLP were spiked into human immunoglobulin G (h-IgG)/100 mM NaCl solution (pH 4.5). Concentrations of h-IgG were 10 mg/ml and 1 mg/ml for Planova 20N and 15N, respectively. Including co-spiking experiments, the MVM spike ratio was determined based on total MVM load to membrane surface area and to be less than 1 v/v% for all filtrations.

2.9 | Immunofluorescence microscopy

After filtration, the filter membranes were collected from the filter housing and fixed in 4% paraformaldehyde phosphate buffer solution overnight at 4°C. The fixed membranes were washed with PBS, cut into small pieces, and embedded in optimal cutting temperature compound (Sakura Finetek Japan Co., Ltd.) at −20°C for sectioning. Cross-sectional 8-μm-thick sections were cut in the direction of filtration using a Leica CM1950 cryostat microtome (Leica Biosystems Nussloch GmbH). Following wash, sections are blocked with 2% bovine serum albumin and PBS containing 0.05% Tween20 (PBS-T) for 10 min at room temperature. Following antibody staining, sections were mounted on glass slides with Vectashield mounting medium (Vector Laboratories, Inc.). Unused membranes were similarly treated and stained as blank experiments.

Immunostained sections were observed by DMi8 system with LAS-X software (Leica Microsystems CMS GmbH). Excitation filter, emission filter, and dichroic mirror wavelength specifications were 480/40, 527/30, and 505 nm, respectively. All samples and blanks were observed under a 100× oil immersion objective lens. Conditions such as exposure time were adjusted in each experiment to obtain enough fluorescence signal. Images were captured using a DFC9000 camera (Leica Microsystems) in 16-bit TIFF format. Fluorescence images collected as z-series spanning the entire section thickness were deconvoluted by LASX software and analyzed using the ImageJ (ver1.52a) Plot Profile tool.

Bright field imaging was also performed to define the inner and outer surface positions. Four linear regions of interest beginning at the inner and ending at the outer surface were selected per image and the fluorescence signal intensity profile across the membrane thickness was analyzed. Signal intensities were normalized relative to a maximum value of 100 and plotted against relative hollow fiber positions with the inner surface as zero and the outer surface as one.

2.10 | Polyacrylamide gel electrophoresis and immunoblotting

Virus analysis by sodium dodecyl sulphate-polyacrylamide gel electrophoresis (SDS-PAGE) was performed using Mini-PROTEAN TGX Precast Gels (10% or 4%–15% Bis-Tris gels; Bio Rad Laboratories, Inc.). Virus samples were mixed with a final 1× Laemmli sample buffer supplemented with 200 mM DTT at a 1× concentration and denatured for 5 min at 95°C.

For silver stain, gels were stained using Pierce Silver Stain Kit (Thermo Fisher Scientific). For immunoblotting, samples in gels were transferred to nitrocellulose membranes using Bio Rad Western Blotting Transfer Systems and detected by chemiluminescence with LAS500 (GE Healthcare, Inc.).

2.11 | Dynamic light scattering

MVM in the storage buffer were measured using Zetasizer Nano ZSP (Malvern Panalytical) and analyzed with Zetasizer Software (Malvern Panalytical). Light intensity at the time of measurement (attenuation setting of the irradiated light), distance from the light source, and total measurement time (number of runs and run duration) were set using the auto-configuration function with setting at room temperature and measurement angle at 173°. Data are shown as the mean of three measurements.

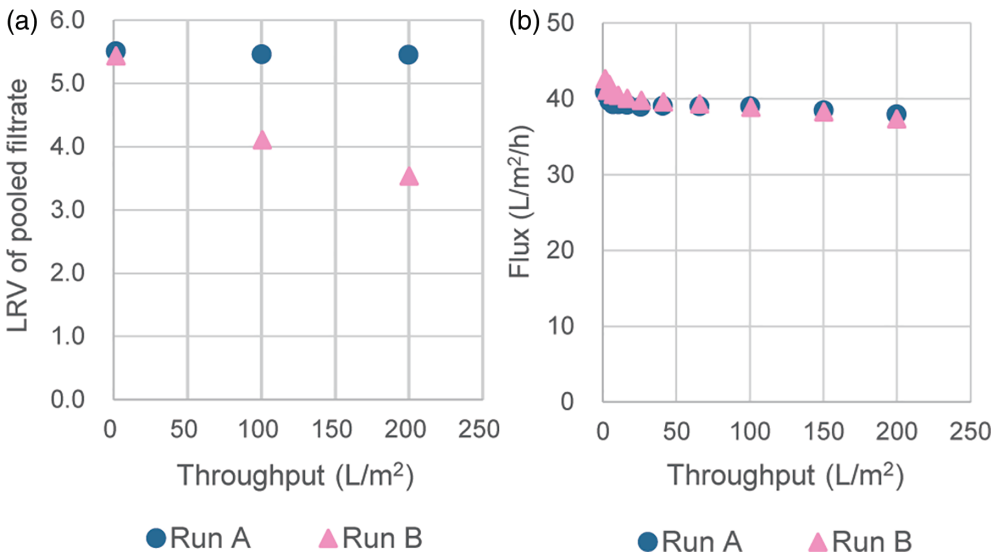

FIGURE 1 Marked differences are observed in virus removability between viral clearance studies with similar designs.(a) Plot of log reduction value (LRV) against throughput (L/m^2) for Runs A and B. A solution of 10 mg/ml human immunoglobulin G/100 mM NaCl (pH 4.5) was spiked with minute virus of mice (MVM) to an infectivity titer of 6.0 $Log_{10}[TCID_{50}/ml]$. On filtration with Planova 20N, filtrate fractions were collected every 0.2 $Log_{10}[copies/m^2]$ (or $Log_{10}[TCID_{50}/m^2]$). Total fraction virus infectivity was measured and pool log reduction values at 100 and 200 L/m^2 were calculated.(B) Plot of flux against throughput (L/m^2) based on the filtration data in (a)

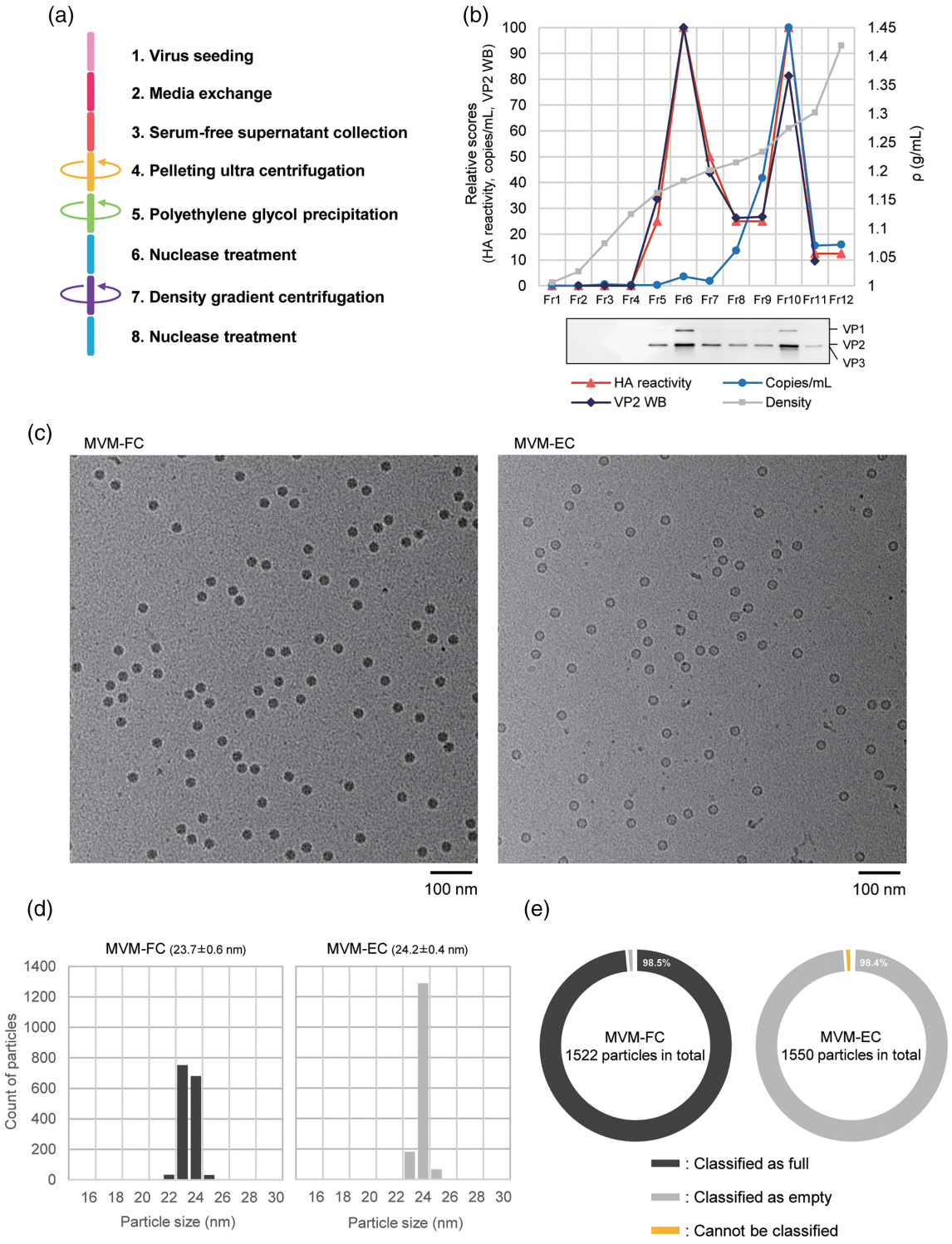

FIGURE 2 Separation of full capsids (FC) and empty capsids (EC) from crude minute virus of mice (MVM). (a) Summary of MVM purification steps. (b) Identification of MVM-FC and -EC in the gradient after centrifugation. Hemagglutination (HA) titer and genomic DNA concentration were measured by HA assay and quantitative polymerase chain reaction, respectively, for all 12 fractions recovered from the top to bottom of the tube. Capsid proteins were also detected by western blotting and VP2 band intensities were measured. Normalized values are plotted on the left axis and fraction density on the right. (c) Cryogenic transmission electron microscopy (cryo-TEM) analysis of MVM-FC and -EC (scale bar, 100 nm). (d) Particle size distribution analysis of cryo-TEM images (mean ± SD). Acquired images were analyzed by Vironova AB using their original imaging and analysis software. (e) Particle classification based on internal density. Acquired images were analyzed by Vironova AB using their original imaging and analysis software

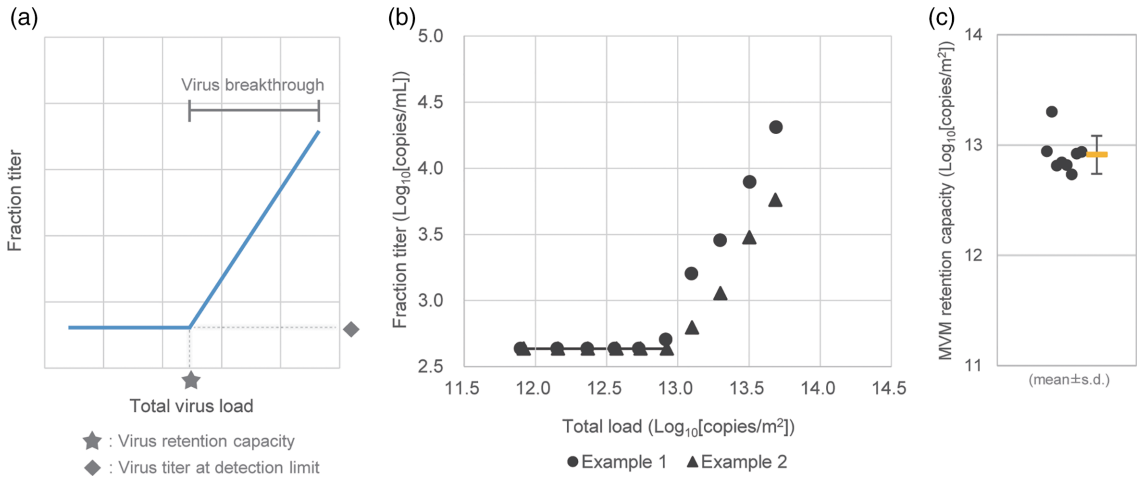

FIGURE 3 Minute virus of mice (MVM) retention capacity of Planova 20N. (a) Graph illustrating virus breakthrough and virus retention capacity. The virus retention capacity of the virus filter is defined as the total virus load at the first filtrate fraction from which virus was continuously detected (star). (b) A solution of 10 mg/ml human immunoglobulin G/100 mM NaCl (pH 4.5) was spiked with MVM and filtered with Planova 20N. Filtrate fractions were collected every 0.2 Log_{10}[copies/m^2] and filtrate and feed solution MVM concentrations were measured using quantitative polymerase chain reaction. Filtrate MVM concentration (Log_{10}[copies/ml]) was plotted against total load (Log_{10}[copies/m^2]). Two example runs are presented here. (c) Plot of MVM retention capacity of Planova 20N

2.12 | Electron microscopy (cryogenic transmission electron microscopy)

Samples were prepared by the authors and cryogenic transmission electron microscopy (cryo-TEM) analysis was performed by Vironova AB. Portions (3 μL) of each sample were applied to a suitable hydrophilized electron microscopy grid such as continuous or holey carbon and subsequently plunge-frozen in liquid ethane. Grids were imaged using a Talos L120C TEM run at 120 kV accelerating voltage. Representative areas were imaged at low and high magnification. Approximately 25 of images were acquired only on grids showing suitable on-grid concentration, particle distribution, and image contrast. Overall sample morphology, size distribution analysis, and particle classification based on internal density were performed by Vironova AB using their original Vironova Imaging and Analysis Software.

3 | RESULTS

3.1 | Marked variability in virus LRV was observed among VCS designed with a comparable feed virus titer

Feed MVM was spiked at concentrations of 6.01 Log_{10}[$TCID_{50}$/ml] (Run A) and 5.94 Log_{10}[$TCID_{50}$/ml] (Run B) and filtered with Planova 20N. The MVM LRV at the 100 and 200 L/m^2 were 5.5 and 5.5, respectively, in Run A and 4.1 and 3.5, respectively, in Run B (Table 1; Figure 1a). While the LRV differed greatly, no major differences in filtration flux were observed between Runs A and B (Figure 1b).

Interestingly, MVM genome counts in the feed solutions of Runs A and B measured by qPCR were 7.21 and 9.18 Log_{10}[copies/ml], respectively (Table 1). There is almost no difference in feed virus infectivity between Runs A and B but approximately 90-fold based on genome number-based titration.

3.2 | Establishment of particle number-based virus clearance study method

The reduction in LRV in Run B of Figure 1 was hypothesized to be due to the large load of virus particles relative to the infectivity. As infectivity does not necessarily reflect the number of particles, the results of infectivity-based and particle number-based evaluations will differ. To test this hypothesis, it is necessary to establish an experimental system capable of quantifying total virus particle number.

Genomic nucleic acid quantification by qPCR was selected to determine parvovirus particle number. When determining total particle number by qPCR, care is required regarding empty particles lacking a target genome. During the parvovirus replication process, genomic DNA is inserted into previously assembled viral capsids.[16–18] Viral capsids into which genomic DNA has not been inserted, in other words, empty particles, cannot be quantified using qPCR. Thus, a qPCR method of measuring the genome copy number in virus stock from which empty particles have been removed (full capsid [FC]-qPCR) was developed as a model system for accurate quantification of particle number. As parvoviruses have one copy of negative-sense DNA per particle, the genome copy number measured by FC-qPCR can be treated as the parvovirus particle number for FC virus stock.

A FC virus stock was prepared based on the various purification methods described in the literature.[14,15] The purification scheme is summarized in Figure 2a. The MVM released into the culture supernatant was concentrated and subjected to iodixanol density gradient

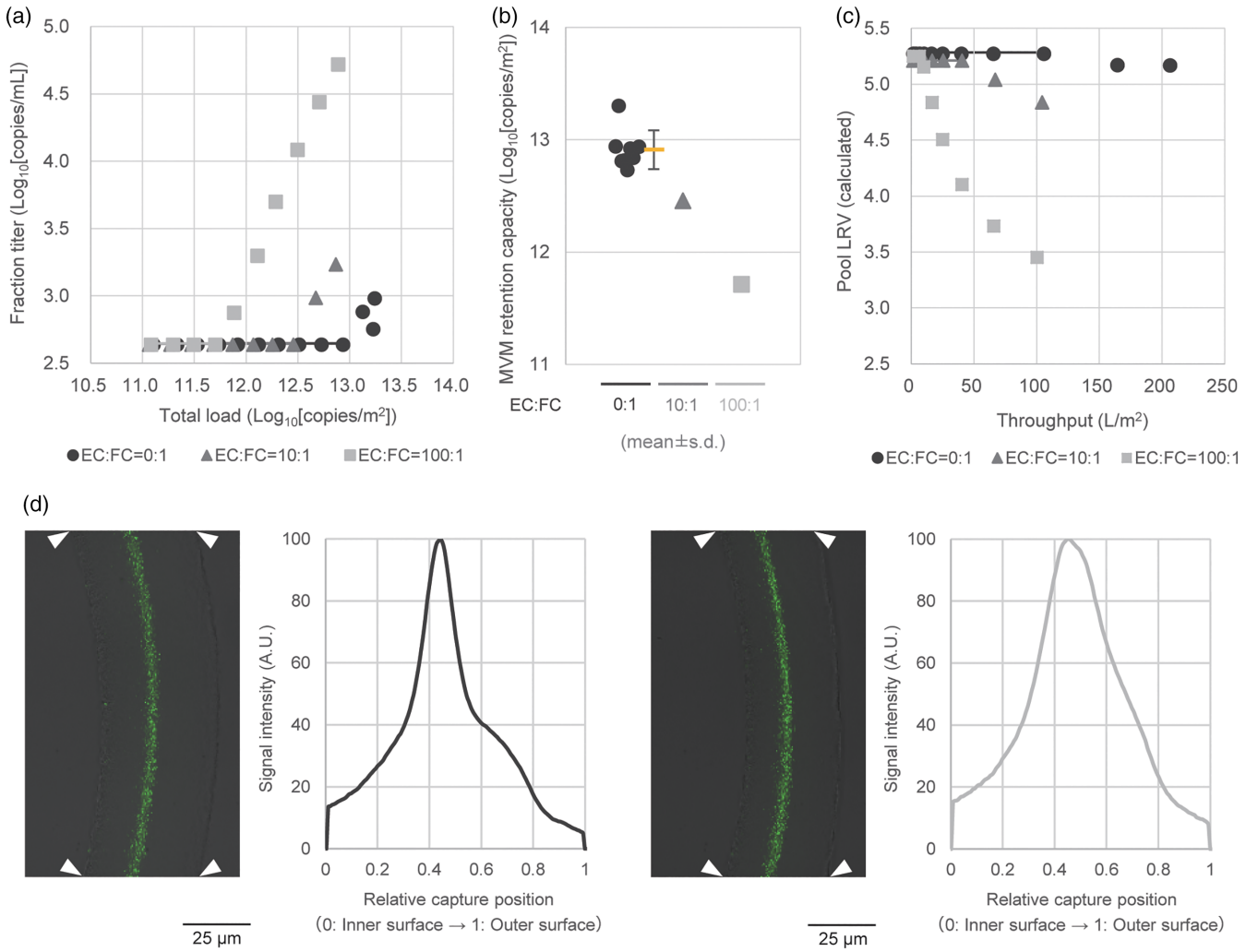

FIGURE 4 Empty capsids (EC) compete with full capsids (FC) for virus retention capacity, causing early virus breakthrough. A solution of 10 mg/ml human immunoglobulin G/100 mM NaCl (pH 4.5) spiked with minute virus of mice (MVM)-FC was co-spiked with MVM-EC at ratios of 10:1 or 100:1 and filtered with Planova 20N. Filtrate fractions were collected every 0.2 Log_{10}[copies/m^2] and filtrate and feed solution MVM concentrations were measured using quantitative polymerase chain reaction. The Planova 20N retention capacity with MVM-FC alone was used a non-co-spiking control (EC:FC = 0:1). (a) Plot of filtrate MVM concentration (Log_{10}[copies/ml]) against total load (Log_{10}[copies/m^2]). (b) The MVM retention capacity of Planova 20N on co-spiking with MVM-EC. (c) Plot of changes in log reduction value against throughput (L/m^2). (d) Solutions separately spiked with MVM-FC and MVM-EC were filtered with Planova 20N and the positions of the virus particles captured in the hollow fiber were detected (scale bar, 25 μm). The inner and outer surfaces of the hollow fibers are indicated by arrow heads. Virus fluorescence signal was quantified and signal distribution was plotted against membrane thickness direction

ultracentrifugation following nuclease treatment. As in previous studies, MVM particles were identified at buoyant densities of close to 1.18 and 1.25 g/ml. Almost no genome was present at the low-density peak while the highest overall proportion of genome was detected at the high-density peak. Furthermore, the genomic DNA detected at the high-density peak was nuclease resistant (i.e., encapsidated DNA). These observations led to the conclusion that the low- and high-density peaks were associated with empty particles (MVM-EC) and genome-containing particles (MVM-FC), respectively.[14,15] The quantity of VP2 protein corresponded to the HA activity peaks (Figure 2b).

Next, MVM-EC and MVM-FC morphologies and degrees of separation were analyzed (Figure 2c). Both virus stocks were examined using cryo-TEM. Approximately 1500 virus particles were examined for each stock and mean particle size and proportion of genome nucleic acid content were calculated. Overall mean particle size was around 24 nm (MVM-FC, 23.7 ± 0.6 nm; MVM-EC, 24.2 ± 0.4 nm [mean ± SD]; Figures 2c, d). As shown in Figure 2e, particle inner region was black for 98.5% of MVM-FC (containing DNA) and white for 98.5% of MVM-EC (empty).

Hydrodynamic diameter, which indicates the sum of capsid and hydration layer, of MVM-FC calculated from the main peak of dynamic light scattering profile (61.5% scatter intensity) was 35.8 nm (Figure S1A), while MVM-FC and MVM-EC were both confirmed by SDS-PAGE to be mainly composed of VP proteins (Figure S1B).

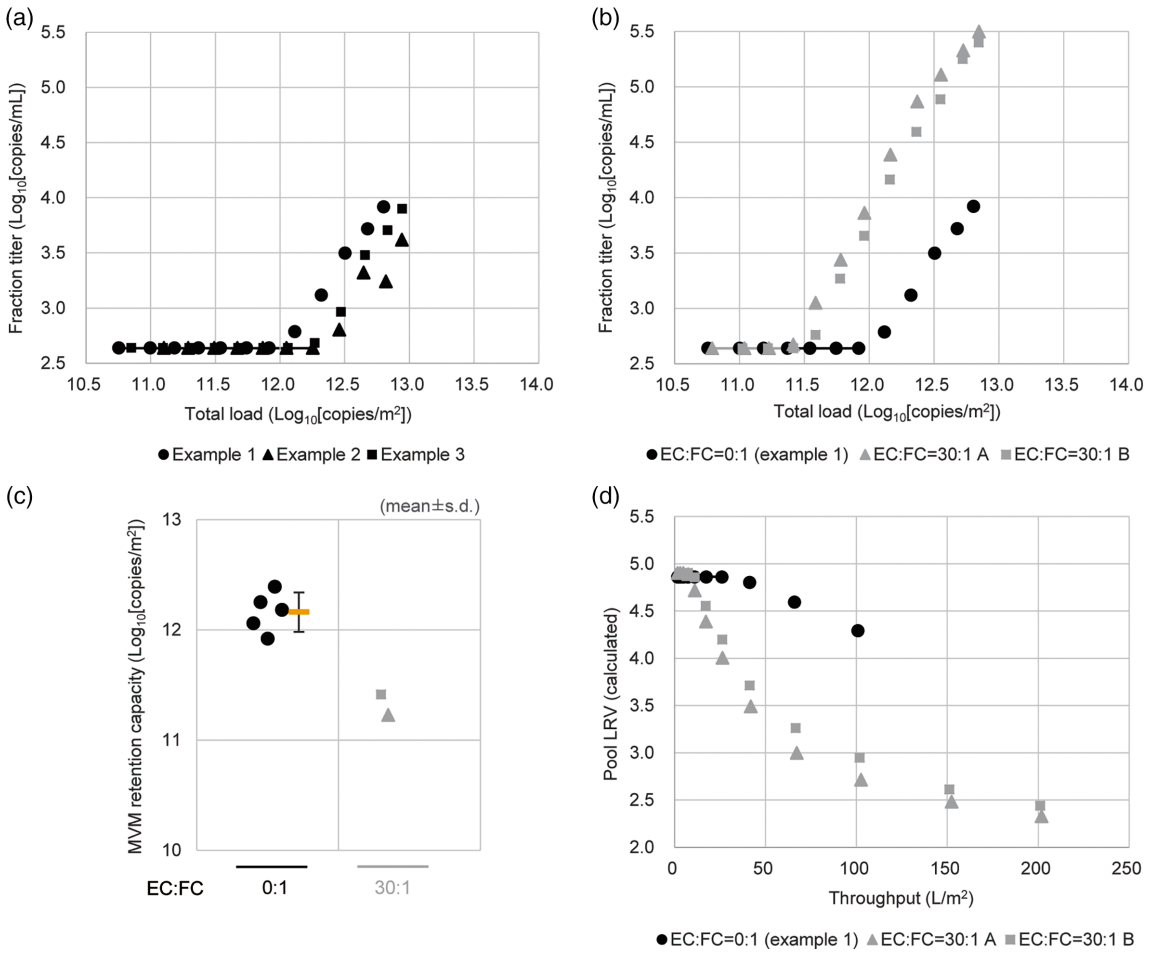

FIGURE 5 Decreased virus retention capacity due to empty particles is a common concern for all types of virus filtration. (a) A solution of 1 mg/ml human immunoglobulin G (h-IgG)/100 mM NaCl (pH 4.5) was spiked with minute virus of mice (MVM) and filtered with Planova 15N. Filtrate fractions were collected every 0.2 Log_{10}[copies/m^2] and filtrate and feed solution MVM concentrations were measured using quantitative polymerase chain reaction (qPCR). Filtrate MVM concentration (Log_{10}[copies/ml]) was plotted against total load (Log_{10}[copies/m^2]). (b) A 1 mg/ml h-IgG/100 mM NaCl (pH 4.5) solution spiked with MVM was co-spiked with MVM-virus-like particles (VLP) at a ratio of 30:1 and filtered with Planova 15N. Filtrate fractions were collected every 0.2 Log_{10}[copies/m^2] and filtrate and feed solution MVM concentrations were measured using qPCR. Filtrate MVM concentration (Log_{10}[copies/ml]) was plotted against total load (Log_{10}[copies/m^2]). (c) Plot of the MVM retention capacities of Planova 15N for MVM-full capsids spiked alone and co-spiked with MVM-empty capsids. (d) Plot of the changes in log reduction value against throughput (L/m^2) for Planova 15N filtration after co-spiking with MVM-VLP (see [b])

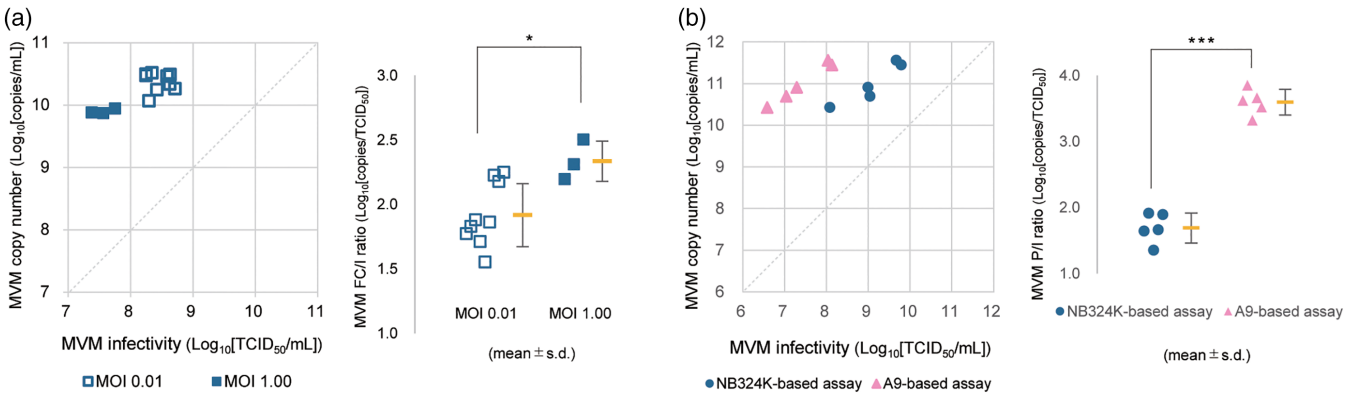

FIGURE 6 (a) Left: Plot of infectivity titer and copy number of MVM propagated at multiplicities of infection (MOI) of 0.01 and 1.00. Infectivities were measured using NB324K cells. Dotted line indicates $y = x$. Right: Scatter plot of MVM FC/I ratio. (b) Left: Plot of infectivity titer measured using NB324K and A9 cells against copy number. The infectivities of five lots of MVM-full capsid stock produced using the same method were measured using NB324K and A9 cells. Dotted line indicates $y = x$. Right: Scatter plot of MVM P/I ratio. *$p < 0.05$; ***$p < 0.001$ by two-tailed Student's t test (a, b)

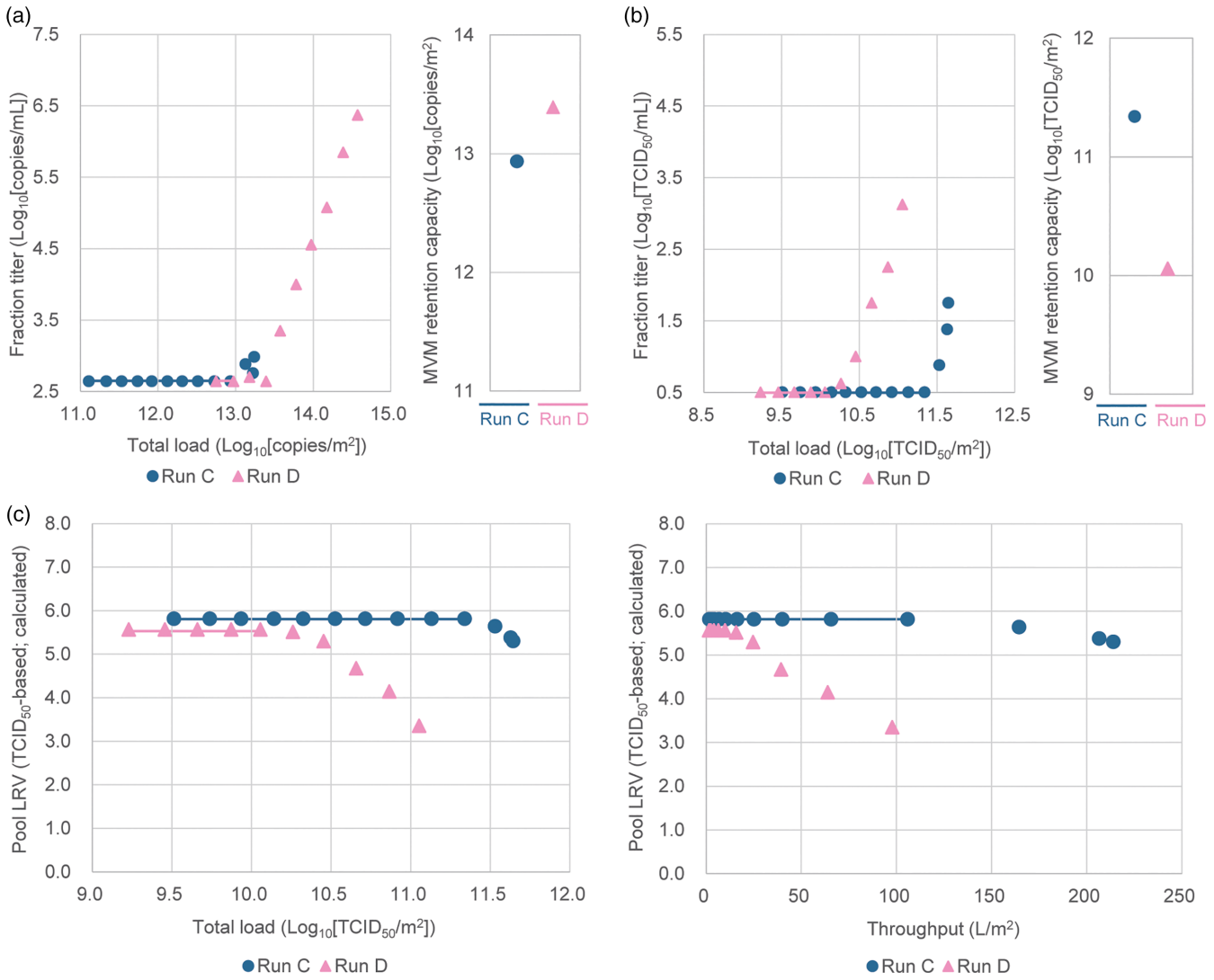

FIGURE 7 Virus overload and early virus breakthrough in evaluation systems with large particle to infectivity (P/I) ratios A solution of 10 mg/ml human immunoglobulin G/100 mM NaCl (pH 4.5) was spiked with minute virus of mice (MVM) to an infectivity titer of 6.0 $Log_{10}[TCID_{50}/ml]$. Total fraction virus infectivity was measured and the decrease in log reduction value (LRV) was calculated from the pool and maximum LRV at 100 L/m^2. (a) The solutions were filtered with Planova 20N and filtrate fractions were collected every 0.2 $Log_{10}[copies/m^2]$ (or $Log_{10}[TCID_{50}/m^2]$). Minute virus of mice retention capacity ($Log_{10}[copies/m^2]$) in Runs C and D and filtrate MVM concentration ($Log_{10}[copies/ml]$) are plotted against total load ($Log_{10}[copies/m^2]$). (b) Minute virus of mice retention capacity ($Log_{10}[TCID_{50}/m^2]$) in Runs C and D and filtrate MVM concentration ($Log_{10}[TCID_{50}/ml]$) are plotted against total load ($Log_{10}[TCID_{50}/m^2]$). (c) Changes in LRV (calculated using infectivity titer) in Runs C and D are plotted against total load ($Log_{10}[TCID_{50}/m^2]$). (d) Changes in LRV (calculated using infectivity titer) in Runs C and D are plotted against throughput (L/m^2)

Planova 20N viral removal performance was evaluated using FC-qPCR. Filtrate fractions were collected at incremental increase of the viral load by +0.2 $Log_{10}[copies/m^2]$, and the virus concentration in each fraction was measured. The virus retention capacity of the VF was defined as the total viral load at the virus breakthrough point, which was defined as the first filtrate fraction from which virus was continuously detected (Figure 3a).

Figure 3b shows example breakthrough curves for Planova 20N. Filtration flux is shown in Figure S2. Planova 20N retention capacity was plotted after repeating the experiment eight times (Figure 3c). Under these conditions, Planova 20N MVM retention capacity was determined to be 12.91 ± 0.17 $Log_{10}[copies/m^2]$ (mean ± SD).

3.3 | MVM empty particles reduce virus retention capacity of VFs

Next, the effects of empty particles on evaluation of VF performance were investigated using MVM-EC co-spiked with FC as 'undetectable' particles for FC-qPCR. The MVM-EC particle number was quantified by HA assay using MVM-FC as a quantification standard. MVM-FC HA titer of $Log_{10}[copies/ml] = 12.05$ was used as the standard to calculate MVM-EC particle number. The MVM-FC copy number used for the filtration test was 12.27 $Log_{10}[copies/ml]$ with an HA titer of ×3200 while the MVM-EC copy number was 9.83 $Log_{10}[copies/ml]$ with an HA titer of ×3200 (Table 2).

Planova 20N MVM-FC retention capacity and LRV changes were observed on quantitative co-spiking of MVM-EC with MVM-FC. Feed solutions comprising h-IgG solution spiked with MVM-FC at a concentration of approximately 8.00 Log_{10}[copies/ml] were further co-spiked with MVM-EC to concentrations of 9.00 and 10.00 Log_{10}[particles/ml] (Figures S3A, B) and filtered with Planova 20N. As in Figure 3b and c, Planova 20N breakthrough curves and MVM retention capacities were plotted for each filtration (Figures 4a, b). Filtration flux and infectivity assay-based analysis are also shown in Figure S3C, D. Compared to spiking with MVM-FC alone, MVM-FC retention capacities on co-spiking with MVM-EC decreased by 0.33 and 0.96 Log_{10} (means of two experiments for initial concentrations 9.00 and 10.00 Log_{10}[particles/ml], respectively). Changes in MVM-FC LRV were plotted against throughput for these filtrations (Figure 4c). The decrease in throughput observed at the onset of LRV decrease was associated with an increase in MVM-EC co-spike ratio. Figure 4b shows the retention capacity decrease at MVM-EC co-spike concentrations of 9.00 (EC:FC = 10:1) and 10.00 (EC:FC = 100:1) Log_{10}[particles/ml].

To investigate the mechanism of decreases in MVM-FC retention capacity and LRV, h-IgG solutions separately spiked with MVM-FC and MVM-EC were filtered with Planova 20 N and the capture positions inside the hollow fibers were analyzed by IF microscopy. After filtering MVM-FC and MVM-EC up to approximately 13.00 Log_{10}[copies/m^2] or 13.00 Log_{10}[Particles/m^2], secondary antibody staining was used to locate virus particles captured in the hollow fiber. Plots of relative fluorescence signal distribution against membrane thickness direction revealed similar peak maximum positions for MVM-FC and MVM-EC at 0.44 and 0.46, respectively (Figure 4d).

The empty particles themselves, rather than other impurities in MVM-EC, were confirmed by co-spiking MVM-FC and MVM-VLP to be responsible for the decrease in virus removal capability (Figures S3E, F).

These results suggest that both detectable virus particles and 'undetectable' empty particles are captured in the same VF pore region. Competitive capture of empty particles in the structures designed to capture detectable virus particles may compete for capacity, decreasing virus removal performance.

The universality of the decrease in the virus removal performance of VF due to empty particles was further investigated. Using Planova 15N, a filter with different characteristics than Planova 20N, MVM retention capacity was evaluated and co-spike experiments were conducted with 'undetectable' empty particles for FC-qPCR.

The MVM retention capacity of Planova 15N was measured using FC-qPCR. Figure 5a shows example breakthrough curves for Planova 15N. Filtration flux is shown in Figure S4A. After repeating the experiment five times, Planova 15N MVM retention capacity was plotted (Figure 5c) and quantified as 12.16 ± 0.18 Log_{10}[copies/m^2] (mean ± SD).

Next, empty particle co-spike experiments were performed as in Figure 4. Feed solution comprising h-IgG solution spiked with MVM-FC at a concentration of approximately 7.50 Log_{10}[copies/ml] was further co-spiked with MVM-VLP to a concentration of 9.00 Log_{10}[particles/ml] and filtered with Planova 15N, and breakthrough curves and MVM retention capacity were plotted (Figure 5b, c). Compared to spiking with MVM-FC alone, MVM-FC retention capacity on co-spiking with MVM-VLP decreased by 0.84 Log_{10} (mean of two experiments). Changes in MVM-FC LRV were also plotted against throughput for these filtrations (Figure 5d). A decrease in the throughput at the onset of LRV decrease accompanied MVM-VLP spiking.

The Planova 15N capture positions for MVM-FC and MVM-VLP were also confirmed by immunofluorescence analysis to be almost the same (Figure S4B).

These results indicate that the decrease in virus retention capacity due to co-spiking of empty particles is a common phenomenon in VF with different membrane structures.

3.4 | Variation in particle to infectivity ratio makes virus retention capacity of VFs looks inconsistent

The investigations in Figures 3–5 clarified that the capacity of VF is constant with respect to the number of particles but overloading with empty particles that competes with genome-containing particles for filter retention capacity makes virus retention looks inconsistent. The important point here is that if the amount of virus load cannot be correctly recognized, the virus removal performance of the VF either cannot correctly evaluated.

In this context, the same problem can occur with VCS, which is evaluated by infectivity. The virus stock might contain viruses that do not have infectivity, and depending on the evaluation system, the infectivity titer may be different even for the same virus stock. The possible presence of such virus particles and variation of infectivity titration in the virus stock can be comprehensively and numerically expressed by the concept of particle-to-infectivity (P/I) ratio.[19] The P/I ratio for a particular virus stock is defined as

$$\text{P/I ratio} = \text{Log}_{10}[(\text{Particle number})/(\text{Infectivity})]. \quad (1)$$

The higher the P/I ratio, the more virus particles will be present for a given infectivity value. Currently, VCS design is usually based on infectivity value alone. Thus, if viruses and/or evaluation systems with

TABLE 1 Marked difference in virus removability between viral clearance studies with similar designs

Run	Feed MVM titer (Log_{10}[$TCID_{50}$/ml])	Feed MVM titer (Log_{10}[copies/ml])	Pooled LRV at 100 L/m^2 ($TCID_{50}$-based, calculated)	Pooled LRV at 200 L/m^2 ($TCID_{50}$-based, calculated)
A	6.01	7.21	5.5	5.5
B	5.94	9.18	4.1	3.5

different P/I ratios are used, the virus concentration in the VF feed solution may differ, even with the same VCS design.

First, we investigated variations in MVM P/I ratio using MVM-FC. For FC virus stock, the number of genomic nucleic acid molecules is equal to the number of virus particles (copies/ml = Particles/ml) so the P/I ratio of FC virus can be replaced by full capsid-to-infectivity (FC/I) ratio. In the present study, FC/I ratio is defined as

$$\mathrm{FC/I\,ratio} = \mathrm{Log_{10}}[(\mathrm{copies/ml})/(\mathrm{TCID_{50}/ml})]. \quad (2)$$

In general, virus P/I or FC/I ratio changes according to the conditions used for virus amplification and harvest; for example, the MOI is known to impact the P/I ratio.[20] Amplification of MVM after changing the MOI resulted in virus stocks with a different FC/I ratio (Figure 6a).

The present study also confirmed that P/I ratio changed depending on the method of quantifying infectivity even when dealing with the same virus. Measurements of $TCID_{50}$/ml for five types of FC virus stock using NB324K or A9 cells resulted in virus infectivity titers approximately 1.70 Log_{10} higher with NB324K than with A9 cells (Figure 6b). Calculating the P/I ratio for each virus stock showed a difference of 1.70 Log_{10} when quantifying infectivity using NB324K compared to A9 cells.

Thus, P/I ratio reflects both the characteristics of the virus stock and differences in titration based on the method of infectivity assay. That is, comparison of P/I ratios elucidates differences between apparent viral load (infectivity) and actual viral load (particle number, genomic nucleic acid copy number in the case of FC virus).

Investigation of the effects of variation in P/I ratio on infectivity-based VCS generated the following findings.

To test the hypothesis that an evaluation system with an extremely high P/I ratio would cause virus overload and early filter breakthrough, VCS based on virus evaluation systems with different P/I ratios were designed.

Based on the $TCID_{50}$/ml values measured with NB324K (Run C) and A9 (Run D) cells, MVM-FC was spiked into h-IgG solution to give a feed solution virus concentration of approximately 6.00 Log_{10}[$TCID_{50}$/ml], the typical concentration of virus spiked into process solution in VCS. The MVM genomic nucleic acid copy concentrations in each feed solution were 7.91 Log_{10}[copies/ml] for the NB324K (P/I ratio = 1.59) and 9.58 Log_{10}[copies/ml] for the A9 (P/I ratio = 3.52) systems (Table 3a). Solutions were filtered through Planova 20N and breakthrough curves plotted based on FC-qPCR demonstrated equivalent MVM retention capacity for both Runs (Figure 7a). Conversely, breakthrough curves plotted based on $TCID_{50}$ assay showed a difference in MVM retention capacity of around 1.00 Log_{10} between the NB324K and A9 systems (Figure 7b). Comparison of $TCID_{50}$ LRV against throughput revealed that LRV decrease began at a lower throughput with the A9 system (Figure 7c) with $TCID_{50}$ LRV at 100 L/m^2 of ≥5.8 and 3.3 for the NB324K and A9 systems, respectively (Table 3b).

While the apparent viral load expressed as $TCID_{50}/m^2$ was almost identical between the A9 and NB324K systems, a difference of at least 1.50 Log_{10} was observed with FC-qPCR. Thus, in filtration designed by large P/I ratio system, overloading of VF capacity likely results in virus breakthrough at a smaller apparent (infectivity-based) viral load.

Virus breakthrough likely occurs when the total number of particles exceeds VF retention capacity (Figure 4). These results confirm the conclusion that variation in P/I ratio makes virus retention capacity of VFs looks inconsistent.

TABLE 2 Minute virus of mice full capsid (FC) and empty capsid (EC) titrations for co-spiking study

Spiking virus	Stock MVM copy number (Log_{10}[copies/ml])	HA titer (x)
MVM-FC	12.27	3200
MVM-EC	9.83	3200

4 | DISCUSSION

The present study demonstrated that empty particles loaded on to VF and variations in P/I ratio of virus stocks make the performance of VF inconsistent even in traditional infectivity-based VCS. Thus, differences in virus stock quality and virus detection methods are important factors for consideration that contract research organizations and VF users when designing studies.

4.1 | Particle number-based VCS

In order to examine how each of the three parvovirus morphologies (infectious, noninfectious, and empty) affected VCS, a virus particle number-based VCS experiment system (FC-qPCR) was developed (Figures 2 and 3).

Performing particle number-based VCS requires a detection sensitivity capable of achieving an LRV comparable to that of infectivity assay. The limit of detection for the FC-qPCR method is 2.64 Log_{10}[copies/ml]. Since the NB324K-based P/I ratios of our MVM are 1.64–2.35 Log_{10} (Figure 6b), the viral nucleic acid concentrations of the 6.00 Log_{10}[$TCID_{50}$/ml] VF feed solution are 7.50–8.00 Log_{10}[copies/ml]. Under these conditions, the maximum possible LRV with FC-qPCR is 4.9–5.4.

4.2 | Virus retention capacity of VF

Using virus retention capacity enables the virus removal performances of VF to be expressed independently of the VCS design. To our knowledge, present study is the first to elucidate particle-number based virus retention capacity of VFs.

The Planova filter hollow fiber membrane comprises a multi-layer structure in which pores consisting of voids and capillaries are connected in a three-dimensional (3D) network. Virus particles are captured in multiple steps as they migrate through the virus retaining pore structures of each layer on their way through the hollow fiber membrane.[21] Particle capture is believed to rely on size exclusion; thus, a smaller pore size should result in a higher virus retention capability. However, with a size exclusion mechanism, the number of virus particles that can be captured in a particular pore structure is limited. On reaching their retention limit, the flow paths in which the virus particles are captured become blocked or reach their retention capacity. If a virus traversing a particular flow path becomes unable to pass through any retaining pore structure, the virus will likely just leak out (while a large number of parvovirus particles, as long as highly purified, rarely cause clogging since sufficient flow path composed of larger pores which do not contribute to virus capture still remain unclogged and maintain flux even when virus retaining pore structure begin to run out). In other words, virus retention capacity corresponds to the viral load at the point that availability of the retaining pore structures decreases to a point that virus is then detected in the filtrate.

Unlike LRV, which is $\log_{10}$ number defining an amount of removed virus, virus retention capacity is not dependent on feed solution virus concentration, only on the capacity within the filter. Therefore, it is likely that evaluations of virus retention capacity more accurately represent the virus removal performance of VF under given solution, temperature, pressure, and other filtration conditions.

VF virus retention capacity evaluated using the approach presented in the present article is strongly influenced by the FC-qPCR virus quantification sensitivity. The higher the detection capability of FC-qPCR, the earlier the timing of virus detection in the filtrate.

The previous study reported that the retention capacity of porcine parvo virus (PPV) was 11.5 ~ 14.4 $Log_{10}[TCID_{50}/m^2]$ for Planova 20N using infectivity assay.[9] We also determined PPV retention capacity using FC-qPCR to be 12.72 ± 0.42 $Log_{10}[copies/m^2]$ (N = 3). While additional data is needed to make a direct comparison, we suppose that the infectivity-based retention capacity of PPV, which is curiously larger than MVM may be explained by its smaller P/I ratio, nearly 0 in our laboratory.

The different membrane structures of the Planova 20N and 15N hollow fibers have different numbers of retaining pore structures,[22] which presumably generates differences in virus retention capacity. The difference in the MVM capture distribution confirms that there are differences between the filters in the membrane pore structures that contribute to virus retention (Figures 4d, S4B). The present findings are consistent with previous reports that the dense layer that contributes to parvovirus retention is wider in Planova 20N than in Planova 15N[22]. The important finding is that empty particles similarly decrease the virus retention capacity of both types of membranes (Figures 4b, 5c). It is assumed that, together with the concept of virus retention capacity, the same effect applies to a wide range of membrane types.

We also note that flux performance of Planova filters were not impacted by particle contents (Figure 1 and S2–S5). This supports that the decreases in retention capacity are effects of competitive capture of empty particles, not of the filter clogging or the flux reduction.

However, it is important to emphasize from the perspective of virus removal performance regarding unknown viruses that parvovirus retention capacity is not an absolute index of VF performance. Parvovirus retention capacity cannot be used to predict removal levels for smaller, unknown viruses. Retention capacity regarding viruses smaller than parvoviruses is expected to correspond to the number of pores smaller than those that capture parvovirus. In other words, from the perspective of safety regarding even smaller viruses, Planova 15N, which has many smaller pores, may have an advantage over Planova 20 N.[23]

4.3 | Effects of empty particles on virus filtration and virus stock quality control strategy

The presence of MVM empty particles reduces the VF virus retention capacity, but the levels of empty particles in virus stocks is currently not routinely evaluated. Industry-wide monitoring of the proportional

TABLE 3 Comparison of viral clearance study design and virus removability using two types of evaluation system with distinctly different particle to infectivity ratios

(A)

Run	Feed MVM Titer (Log_{10}[copies/ml])	Feed MVM titer ($Log_{10}[TCID_{50}/ml]$, NB324K-based)	Feed MVM titer ($Log_{10}[TCID_{50}/ml]$, A9-based)	P/I ratio
C	7.91	6.32	—	1.59
D	9.58	—	6.06	3.52

(B)

Run	Cell line	Maximum LRV	Pooled LRV at 100 L/m^2 ($TCID_{50}$-based, calculated)	LRV reduction at 100 L/m^2 ($TCID_{50}$-based)
C	NB324K	5.8	≥5.8	0
D	A9	5.6	3.3	2.3

contents of empty particles in virus stock is required together with discussion of the impacts.

The present study used a breakthrough curve shift to model and quantitatively consider this phenomenon (Figure 8).

We assume there is no bias in capture rate between FC and empty particles since the slope of the breakthrough curve remained constant (approximately 1.8) regardless of the empty particle spike ratio (Figure 4a).

Assuming that the FC virus and empty particles are identical regarding VF, the breakthrough curves based on total particle number should perfectly overlap in VCS with FC virus alone (VCS α) and VCS with co-spiked empty particles at +c Log_{10} with respect to FC virus (VCS β) (Figure 8, left). The ratio of FC virus to total particle number in VCS β is $1/10^c$, the FC viral load on reaching filter breakthrough point is smaller than that in VCS α by c Log_{10}[copies/m^2]. Furthermore, the concentration of FC virus breakthrough at a certain total particle load is c Log_{10}[copies/ml] smaller than that in VCS α. In other words, replacing the total particle breakthrough curve with breakthrough curves based on FC virus copy number results in equilibrium shift of -c Log_{10} in both the x and y axis directions in VCS β (Figure 8, right). If the breakthrough curve in a general system after filter breakthrough is $y = ax - b$, the breakthrough curve in VCS including c Log_{10} empty particles can be expressed as $y + c = a(x + c) - b$. Since the virus retention capacity is the intersection of the breakthrough curve and $y =$ LoD, the retention capacity A of VCS α and β can be expressed as follows:

$$A_\alpha = (\mathrm{LoD} + b)/a. \quad (3)$$

$$A_\beta = (\mathrm{LoD} + b - c(a-1))/a. \quad (4)$$

In this case, the decrease in retention capacity is expressed as

$$A_\alpha - A_\beta = c(a-1)/a. \quad (5)$$

Thus, FC virus retention capacity in VCS β decreases by c(a - 1)/a [copies/m^2].

In Figure 4, measured and mathematical model values for virus retention capacity decreases are 0.48 and 0.44 Log_{10}[copies/m^2], respectively, for $c = 1.0$; 1.23 and 0.89, respectively, for $c = 2.0$; and 0.81 and 0.67, respectively, for $c = 1.5$ (with MVM-VLP).

The divergence between the measured and mathematical model values might be explained by the effect of impurities contained in the co-spiked MVM-EC (Figure S1B) or minor differences in 3D particle structures of MVM-FC and MVM-EC.[10,24,25]

According to the mathematical model, even preliminarily and more works still needed to validate, retention capacity decreases due to empty particles become evident only when empty particles are present at a 'reasonable' concentration. In the case of Planova 20N, considering the slope of the breakthrough curve (approximately 1.8) and the accuracy of virus retention capacity measurement ($\sigma = 0.17$ Log_{10}), the proportion of empty particle content for which the decrease in retention capacity exceeds an error range of 1.0 σ is estimated to be approximately $c \geq 0.8$. The proportional content of empty particles obtained using our standard MVM production method, which is based on NB324K cells, is $c \leq 0.8$ for most lots (data not shown). Therefore, the risk of a problematic decrease in VF retention capacity due to empty particles is not that high in our laboratory. However, there are no industry-wide standardized methods of virus production for VCS and the proportional content of empty particles may differ among laboratories. Monitoring of this parameter by multiple laboratories is required to investigate the level of impact of decreased VF virus retention capacity due to empty particles. Observations of proportional content of empty particles exceeding $c = 0.8$ should result in the introduction of industry-wide virus quality control focusing on empty particle content.

4.4 | Effects of particle-to-infectivity ratio on virus filtration

As well as empty particles, also in infectivity-based analysis, a discrepancy with total virus particle number and apparent virus amount cause inconsistency VCS result. It is necessary to recognize that virus stock quality and viral titration methods affect particle to infectivity (P/I) ratio.

We used both NB324K and A9 cells as host cells for MVM titration. Previous report showed that MVMp is more sensitively detected in infectivity assay by NB324K cells than A9 cells.[26,27] Our infectivity assay protocol is optimized for each type of host cell, however, a difference of approximately 1.70 Log_{10} was observed in $TCID_{50}$/ml (Figure 6b), consistent with these reports.

This 1.70 Log_{10} difference translates into a higher virus particle concentration used for the VCS (in other words, the higher the P/I ratio in the evaluation system), the smaller the throughput (or viral load as expressed by the infectivity value) at the point filter breakthrough is reached, even for the same apparent viral load (infectivity value). This finding shows that in VCS design based on the infectivity value, filter breakthrough caused by virus overloading occurs at an earlier stage in evaluation systems with high rather than low P/I ratios.

If the P/I ratio is regarded as the difference indicator between the apparent and actual virus load, the same mechanism with empty particles, breakthrough curve shift model applies. The effects of discrepancy between infectivity titer and total particle number can be modeled by replacing c in Equations (4) and (5) with P/I ratio.

The level of impact this phenomenon on the biopharmaceutical industry depends on variety of P/I ratios in the industry. In addition to MOI at virus production, virus inactivation may also alter the P/I ratio. Furthermore, the sensitivity of the infectivity assay system depends not only on the type of host cell but also on the effects of the seeding concentration of cells and virus, culture duration, and reagents such as FBS. Interestingly, previous study demonstrated considerable variability in P/I ratio (almost 2.0 Log_{10} between the highest and the lowest) among commercial virus stocks.[12]

Besides the scientific aspects, these findings also can contribute to optimize manufacturing costs for a VF process of given product. In Run D, with large P/I ratio, pooled LRV became smaller than 4.0 Log_{10}, generally required value for VF process, at less than 100 L/m^2 process volume whereas more than 5.0 Log_{10} of pooled LRV was still observed at 200 L/m^2 in Run C, with small P/I ratio. With the conditions like Run D, VCS based on apparent virus count could

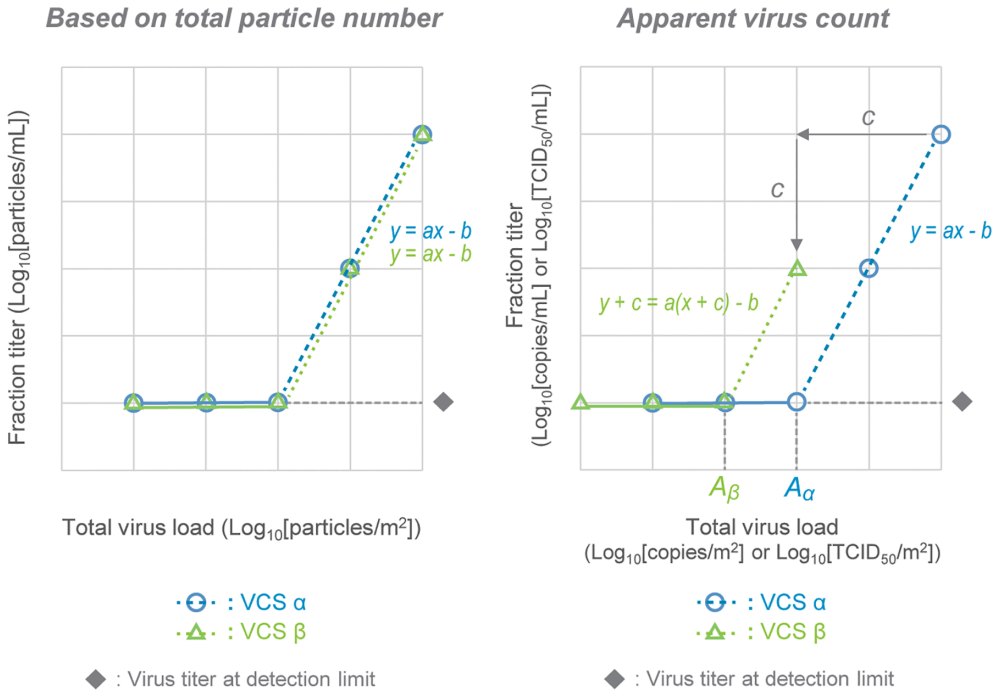

FIGURE 8 Breakthrough curve shift modeling to compare the particle number-based analysis and apparent virus count-based analysis Virus filter breakthrough curves of two virtual virus clearance studies VCS α and VCS β are plotted based on total particle number (left) and apparent virus count (right). Breakthrough curves are fitted by linear, x-axis; Total virus load, y-axis; Fraction titer, Aα; the retention capacity of VCS α, Aβ; the retention capacity of VCS β, a; slope of breakthrough curve, b; value of y-intercept, c; Logarithmic ratio of empty particles for quantitative PCR titration or P/I ratio for infectivity-based titration

significantly limit the process volume per filter and rise the manufacturing cost for a given product because of earlier LRV reduction. By focusing on actual total virus load and designing VCS to avoid overloading, process volume with sufficient LRV can be maximized.

Although additional study regarding the effects of impurities or types of solutions is required, our results highlight that the total particle count has large impact on the interpretation of VF performances and for efforts to optimize VF process in the biopharmaceutical industry.

5 | CONCLUSION

Virus particle number and virus retention capacity should be considered to understand and/or optimize VF performance.

5.1 | Virus particle number

With a conventional VCS approach based on infectivity titer, although the viral load calculated from the infectivity titer is the same, the actual virus particle number in the VF could be different. Therefore, the throughput (L/m^2) that exceeds the retention capacity also differs, resulting in inconsistent LRV for the given solution volume among the identical VCS designs.

While any method of particle counting is acceptable, low-cost solution to avoid these issues can be industry-wide monitoring of P/I ratio and implementation of P/I ratio as a quality control indicator for virus stock manufacturing. Another idea involves adoption of particle-number based VCS methods (e.g., FC-PCR); however, considering its high working cost and unverified site-to-site reproducibility, more work is needed to gain an acceptance within the industry.

5.2 | Virus retention capacity

With a VCS design only focusing on LRV, it was difficult to accurately predict the result for new VCSs from existing data due to lack of consistency in virus concentrations of feed solutions. Here, we propose more robust VCS design method; back-calculation from virus retention capacity.

For example, under operating conditions with large process volumes per production batch, setting the virus concentration to be spiked into the feed solution at 6.00 $Log_{10}[TCID_{50}/ml]$ results in a viral load that exceeds the VF virus retention capacity before the target protein processing quantity is reached, causing filter breakthrough. Intentionally setting the virus concentration to be spiked into the feed solution at a lower level (e.g., around 5.00 $Log_{10}[TCID_{50}/ml]$) reduces the maximum LRV (from 5.5 to around 4.5) while maintaining sufficient virus removal performance so that filtration of the entire batch can be completed without filter breakthrough and keep the required LRV value for the VF process.

In summary, particle number-based analysis and retention capacity-based VCS design would bring the following advantages:

1. Making VCS results inter-facility or -laboratory comparable by avoiding LRV inconsistency among apparently identical VCS designs caused by misidentification of the total virus particles.
2. Achieving robust and cost-effective manufacturing process by identifying the real virus retention capacity of VFs in VCS and back-calculation.

ACKNOWLEDGMENTS

We thank Dr. Andy Bailey of ViruSure GmbH for expert support with this study, and Dr. Johannes Blümel of Paul-Ehrlich-Institut for valuable discussion. We also thank Dr. Daniel Strauss of Asahi Kasei Bioprocess America, Inc. for critical reading and Joanne DeWitt for translation and editing of the manuscript. We gratefully acknowledge Yoshiyuki Sawamura, Mio Akutsu, Chihiro Kato and Naoto Watanabe for valuable assistance in many phases of the study, and Aki Miura and Dr. Takuma Iwasaki for sharing α-MVM mAb and excellent technical assistance with IF microscopy.

AUTHOR CONTRIBUTIONS

Taiki Kayukawa: Conceptualization (lead); formal analysis (equal); investigation (equal); methodology (lead); validation (equal); writing – original draft (equal). **Akiyo Yanagibashi:** Investigation (equal); methodology (supporting). **Tomoko Hongo-Hirasaki:** Writing – review and editing (lead). **Koichiro Yanagida:** Conceptualization (supporting); project administration (equal); writing – review and editing (supporting).

PEER REVIEW

The peer review history for this article is available at https://publons.com/publon/10.1002/btpr.3237.

DATA AVAILABILITY STATEMENT

Data available on request from the authors.

ORCID

Taiki Kayukawa https://orcid.org/0000-0002-0065-4894
Tomoko Hongo-Hirasaki https://orcid.org/0000-0002-6710-044X

REFERENCES

1. Barone PW, Wiebe ME, Springs SL, et al. Implications for emerging therapies. *Nat Biotechnol*. 2020;38:563-572. doi:10.1038/s41587-020-0507-2
2. ICH Harmonized Tripartite Guideline Q5A (R1). Viral safety evaluation of biotechnology products derived from cell lines of human or animal origin. *US Fed Reg*. 1999;63(185):51074.
3. Guideline on virus safety evaluation of biotechnological investigational medicinal products. *EMA* 2008: EMEA/CHMP/BWP/398498/2005;1–9.
4. Sterilizing filtration of liquids task force. sterilizing filtration of liquids. technical report no. 26 (revised 2008). *PDA J Pharm Sci Technol*. 2008; 62(26):2-60.
5. Lute S, Bailey M, Combs J, Sukumar M, Brorson K. Phage passage after extended processing in small-virus-retentive filters. *Biotechnol Appl Biochem*. 2007;47(3):141-151. doi:10.1042/BA20060254
6. Burnham M, Schwartz A, Vyas E, et al. Advanced viral clearance study design: a total viral challenge approach to virus filtration. *Bioprocess Int*. 2018;16(3):52-57.
7. Tsurumi T, Sato T, Osawa N, et al. Mechanism of removing monodisperse gold particles from a suspension using cuprammonium regenerated cellulose hollow fiber (bmm hollow fiber). *Polym J*. 1990; 22(12):1085-1100. doi:10.1295/polymj.22.1085
8. PDA Technical Report No 47. Preparation of virus spikes used for virus clearance studies. *PDA*. 2010;1–63.
9. Hongo-Hirasaki T, Yamaguchi K, Yanagida K, et al. Effects of varying virus-spiking conditions on a virus-removal filter Planova™ 20N in a virus validation study of antibody solutions. *Biotechnol Prog*. 2011; 27(1):162-169. doi:10.1002/btpr.533
10. Cotmore SF, Tattersall P. Parvoviruses: small does not mean simple. *Annu Rev Virol*. 2014;1(1):517-537. doi:10.1146/annurev-virology-031413-085444
11. Tullis GE, Burger LR, Pintel DJ. The minor capsid protein VP1 of the autonomous parvovirus minute virus of mice is dispensable for encapsidation of progeny single-stranded DNA but is required for infectivity. *J Virol*. 1993;67(1):131-141. doi:10.1128/jvi.67.1.131-141.1993
12. Miesegaes G, Lute S, Dement-Brown J, et al. A survey of quality attributes of virus spike preparations used in clearance studies. *PDA J Pharm Sci Technol*. 2012;66(5):420-433. doi:10.5731/pdajpst.2012.00879
13. Hernando E, Llamas-Saiz AL, Foces-Foces C, et al. Biochemical and physical characterization of parvovirus minute virus of mice virus-like particles. *Virology*. 2000;267(2):299-309. doi:10.1006/viro.1999.0123
14. Cotmore SF, Tattersall P. Encapsidation of minute virus of mice DNA: aspects of the translocation mechanism revealed by the structure of partially packaged genomes. *Virology*. 2005;336(1):100-112. doi: 10.1016/j.virol.2005.03.007
15. Wolfisberg R, Kempf C, Ros C. Late maturation steps preceding selective nuclear export and egress of progeny parvovirus. *J Virol*. 2016; 90(11):5462-5474. doi:10.1128/JVI.02967-15
16. D'Abramo AM, Ali AA, Wang F, Cotmore SF, Tattersall P. Host range mutants of minute virus of mice with a single VP2 amino acid change require additional silent mutations that regulate NS2 accumulation. *Virology*. 2005;340(1):143-154. doi:10.1016/j.virol.2005.06.019
17. Richards R, Linser P, Armentrout RW. Kinetics of assembly of a parvovirus, minute virus of mice, in synchronized rat brain cells. *J Virol*. 1977;22(3):778-793. doi:10.1128/jvi.22.3.778-793.1977
18. King JA, Dubielzig R, Grimm D, Kleinschmidt JA. DNA helicase-mediated packaging of adeno-associated virus type 2 genomes into preformed capsids. *EMBO J*. 2001;20(12):3282-3291. doi: 10.1093/emboj/20.12.3282
19. Lang SI, Boelz S, Stroh-Dege AY, Rommelaere J, Dinsart C, Cornelis JJ. The infectivity and lytic activity of minute virus of mice wild-type and derived vector particles are strikingly different. *J Virol*. 2005;79(1):289-298. doi:10.1128/JVI.79.1.289-298.2005
20. Bora M, Yousuf RW, Dhar P, et al. Characterization of defective interfering (DI) particles of *Pestedes petitsruminants* vaccine *virus Sungri/96* strain-implications in vaccine upscaling. *Biologicals*. 2019;62:57-64. doi:10.1016/j.biologicals.2019.09.008
21. Tsurumi T, Sato T, Osawa N, et al. Structure and filtration performances of improved cuprammonium regenerated cellulose hollow fiber (improved BMM hollow fiber) for virus removal. *Polym J*. 1990; 22(12):1085-1100. doi:10.1295/polymj.22.1085
22. Adan-Kubo J, Tsujikawa M, Takahashi K, Hongo-Hirasaki T, Sakai K. Microscopic visualization of virus removal by dedicated filters used in biopharmaceutical processing: impact of membrane structure and localization of captured virus particles. *Biotechnol Prog*. 2019;35: e2875. doi:10.1002/btpr.2875
23. Nowak T, Popp B, Roth NJ. Choice of parvovirus model for validation studies influences the interpretation of the effectiveness of a virus filtration step. *Biologicals*. 2019;60:85-92. doi:10.1016/j.biologicals.2019.04.003
24. Maroto B, Valle N, Saffrich R, Almendral JM. Nuclear export of the nonenveloped parvovirus virion is directed by an unordered protein signal exposed on the capsid surface. *J Virol*. 2004;78(19):10685-10694. doi:10.1128/JVI.78.19.10685-10694.2004
25. Sánchez-Martínez C, Grueso E, Carroll M, Rommelaere J, Almendral JM. Essential role of the unordered VP2 n-terminal domain of the parvovirus MVM capsid in nuclear assembly and endosomal enlargement of the virion fivefold channel for cell entry. *Virology*. 2012;432(1):45-56. doi:10.1016/j.virol.2012.05.025
26. Tattersall P, Bratton J. Reciprocal productive and restrictive virus-cell interactions of immunosuppressive and prototype strains of minute virus of mice. *J Virol*. 1983;46(3):944-955. doi: 10.1128/jvi.46.3.944-955.198327

27. Ball-Goodrich LJ, Tattersall P. Two amino acid substitutions within the capsid are coordinately required for acquisition of fibrotropism by the lymphotropic strain of minute virus of mice. *J Virol*. 1992;66(6): 3415-3423. doi:10.1128/jvi.66.6.3415-3423.1992

SUPPORTING INFORMATION

Additional supporting information may be found in the online version of the article at the publisher's website.

How to cite this article: Kayukawa T, Yanagibashi A, Hongo-Hirasaki T, Yanagida K. Particle-based analysis elucidates the real retention capacities of virus filters and enables optimal virus clearance study design with evaluation systems of diverse virological characteristics. *Biotechnol. Prog*. 2022;38(2):e3237. doi:10.1002/btpr.3237